J. Chem. Sci. (2020)132:37
https://doi.org/10.1007/s12039-020-1739-x

REGULAR ARTICLE

A new Keggin-based organic-inorganic nanohybrid in the role of a dual-purpose catalyst

ALI JAMSHIDI[a,b,*], FARROKHZAD MOHAMMADI ZONOZ[a,*] and YONGGE WEI[c]
[a]Department of Chemistry, Hakim Sabzevari University, Sabzevar 96179-76487, Iran
[b]Young Researchers and Elite Club, Mashhad Branch, Islamic Azad University, Mashhad, Iran
[c]Department of Chemistry, Tsinghua University, Beijing 100084, China
E-mail: jamshidi_ali1982@yahoo.com; fzmohamadi@yahoo.com

MS received 28 August 2019; revised 19 October 2019; accepted 22 October 2019

Abstract. A new organic-inorganic hybrid consisting of Keggin-type polyoxometalate ($[BW_{12}O_{40}]^{5-}$) and protonated piperazine, namely $[H_5O_2]_2[Hpip]_{2.5}[BW_{12}O_{40}]\cdot 4H_2O$ (pip = piperazine, $C_4H_{10}N_2$) (**1**), has been created under reflux state and identified through material identification devices like single-crystal crystallography, FT-IR and ^{1}H-NMR spectroscopies, Powder XRD, TG-DT Analysis, Field Emission SEM, elemental-analysis and cyclic voltammetry. Crystallography investigation exhibits that the main factor in the formation of **1** is the numerous number of hydrogen bonding between organic and inorganic species. The arrangement of Hpip groups creates holes in which the $[BW_{12}O_{40}]^{5-}$ clusters fit into the holes. Furthermore, the electrochemical and photochemical attributes of **1** have been considered, and the outcomes present that **1** owns privileged electrocatalytic activity against the reduction of nitrite ions as well as an appropriate photochemical effect on methylene blue (MB) dye depredation.

Keywords. nanohybrid; Keggin; crystallography; electrocatalyst; photocatalyst.

1. Introduction

Supramolecular compounds have drawn remarkable consideration because they have a significant property like supramolecular gathering which is caused the expanse of low-dimensional components to high-dimensional structures. This structure extension occurs because of feeble intermolecular or intramolecular forces including hydrogen-bonds, π···π stacking, van der Waals attraction and electrostatic interactions.[1] Among various supramolecular materials, polyoxometalates (POMs) are a great category of distinct nanoscaled metal oxide clusters which are consistent of early transition metals such as V, Mo, W, etc., (generally in their highest oxidation states), and they have abundant ending and bridging oxygen atoms which could apply coordination transferors actively to incorporate with diverse metallic ions. Thus, POMs provide forcefully electronegative oxygen atoms to create supramolecular compounds by hydrogen bond forces.[2] Moreover, POMs exhibit a varied kind of anionic molecular types accompanying excessive negative charge, big molar mass, and appropriate solubility in polar solvents.[3] These compounds have considerable attributes and great performance in multiple domains like anti-cancer activity,[4] catalysis,[5] electrochemistry,[6] proton conduction,[7] separation materials,[8] electronic,[9] optical[10] and magnetism.[11] In addition, the classic polyoxoanions with high charge density and major sizes, containing Keggin, Well-Dawson, Linqvist, and so on, have been broadly applied as inorganic building units to build POM-based frameworks. Among the various class of heteropolyanions, the usage of Keggin-type structure as homogenous catalysts have been extensively considered for oxidative type,[12] electrochemistry[13] and photocatalysis[14] reactions. Since, this type of POMs have incomparable features, such as Brønsted acids (more active than the conventional solid acids), and also quick and reciprocal multi-electron redox reaction partly rather moderate conditions.[15] Taking into consideration, due to the noticeable disadvantages of homogeneous catalysis system like the strict recycling of catalysts and products refinement, finding a way to

*For correspondence

Electronic supplementary material: The online version of this article (https://doi.org/10.1007/s12039-020-1739-x) contains supplementary material, which is available to authorized users.

Published online: 07 February 2020

prepare an insoluble POM catalyst has enticed much consideration. There are several ways to synthesize heterogeneous POM catalysts such as locating POMs in porous substrates such as Zeolitic imidazolate frameworks (ZIFs),[16] Santa Barbara Amorphous-15 (SBA-15),[17] KIT-6 silica–polydimethylsiloxane (PDMS),[18] etc., and on nanosized surfaces like Fe_3O[4,19] ZnO,[14] Graphen Oxide,[20] Graphitic carbon nitride (g-C_3N_4)[21] and so on. Among these sample of POMs solidification, the most commonly applied way to construct insoluble POM is the planning and preparing of organic-inorganic hybrid based on POMs (OIH-POMs). Generally, OIH-POMs have been prepared in both noncrystal or crystalline forms in different conditions such as room temperature,[22] reflux[23,24] and hydrothermal (solvothermal) conditions.[25] Since the appearance of OIH-POMs, two kinds of category have been suggested according to how inorganic and organic moieties are bonded together. Firstly, organic and inorganic counterparts are bonded together without any covalent bond and the only factor that causes the connection between POMs and organic species is weak molecular interactions. For example, $[Zn(Hfcz)(H_2O)_3](H_3fcz)(SiMo_{12}O_{40})\cdot 3H_2O$,$(C_6H_6N_3)_7(PMo^{VI}_{12}O_{40})(PMo^{V}Mo^{VI}_{11}O_{40})\cdot 2CH_2$ OH·$5H_2O$, $(H_2bimyb)_3(As_2$ $Mo_{18}O_{62})$, $[CoH_4EDTA(H_2O)]_2(SiW_{12}O_{40})]\cdot 15H_2O$ and so forth.[26–29] In the second category, the organic and inorganic counterparts are tightly bonded together due to the covalent bonding formed by the bridge between the organic and inorganic material by bridging the transition metals. For instance, $[Zn_{12.5}(trz)_{17}(H_2O)_7(SiW_{12}O_{40})_2]\cdot 2H_2O$, $[Cu(Dione)_2(H_2O)]_2(SiW_{12}O_{40})$, $[N(CH_3)_4]_6[Cu^{II}Lo][(Ti_2O)(PW_{11}O_{39})_2]\cdot 4H_2O$, $[Cu(dap)_2]_{3.5}$ $[Cu(dap)_2(H_2O)]_3[La(\alpha SiW_{11}O_{39})_2]\cdot 5H_2O$ and so on.[30–33] Usually, in OIH-POMs materials, the organic ligand is used as nitrogenous because nitrogen plays a crucial role in connection either through weak interactions or through covalent bonds. The protonation of nitrogenous groups in acidic environment and the transformation of them to cationic form supplies an extremely suitable condition for hydrogen bonding among cationic nitrogenous ligands and POM anionic clusters, and also cationic nitrogenous ligands can act as an appropriate electron donor to make covalent bond by sharing their electron pairs to the empty orbitals of adjacent metals.[34,35] In view of the OIH-POMs importance which is already aforesaid, lately we have thus initiated an investigation on the reaction of protonated pip (Scheme 1) and Keggin POMs. In this work, a nano OIH-POMs, scilicet $[H_5O_2]_2$ $[Hpip]_{2.5}[BW_{12}O_{40}]$-$4H_2O$ has been successfully obtained under the reflux condition. This hybrid compound is self-assembled based on hydrogen bonding interactions among $[BW_{12}O_{40}]^{5-}$ anions and Hpip counter ions. Beside the preparation and characterization of **1**, the electrocatalytical property and photochemical activity of this hybrid was studied.

2. Experimental

2.1 *Materials and physical methods*

To identify compound **1**, various instrumental analysis have been used as follows: Themo Finnigan Flash-1112 EA Microanalyzer CHN elemental analyzer and Integra XL Inductively Coupled Plasma Spectrometer (Elemental analyses), Alpha FT-IR spectrophotometer using a KBr pellet in 400–4000 cm^{-1} range (FT-IR spectra), Photonix UV-visible array spectrophotometer (UV-Vis spectra), Brucker BRX-500 AVANCE Spectrometer (NMR spectrum), XPert MPD diffractometer with Cu Kα radiation at 40 keV and 30 mA (scanning rate was 3° min^{-1} in the range of 5°–80°; powder X-ray diffraction), HITACHI S-4160 with gold coating (FESEM) and TGA-50 Shimadzu thermal analyzer under N_2 atmosphere with the heating rate of 10 °C min^{-1} in the range of 30–700 °C (Thermogravimetric analyses). In electrochemistry evaluation, a Millipore Q water filtration device was acquired to obtain distilled water by passing through this device. The reaction media was subjected to nitrogen gas passage for 25 min and was subjected to a nitrogen atmosphere for the entire duration of the experiment. The electrochemical instrument used in this investigation was Metrohm 797 VA polarographic analyzer. In this electrochemical system, three-electrode was utilized as follows: the modified CPE (working electrode), a platinum electrode (counter electrode) and an Ag/AgCl (3 M KCl, reference electrode). All potentials were measured, evaluated and announced based on the Ag/AgCl electrode. All voltammetric tests were performed at room temperature. The 0.5 M buffer solutions of Na_2SO_4/H_2SO_4 for electrochemical checking were prepared by the combination of diverse amounts of related acid and sault.[36]

2.2 *$[H_5O_2]_2$ $[Hpip]_{2.5}[BW_{12}O_{40}]\cdot 4H_2O$ synthesis*

pip (0.058 g) was dissolved in 10 mL HCl (1M) and added drop by drop to a solution of $H_5[\alpha$-$BW_{12}O_{40}]$-nH_2O (0.18 g, in 50 mL distilled water) in steady stirring mode. The resulting clear solution was warmed moderately until 90 °C and maintained for 5 h at stirred and reflux conditions. After a month, clear colorless irregular crystalline solids were manually

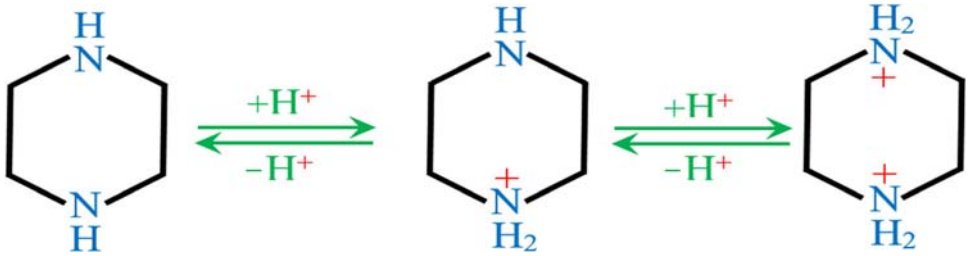

Scheme 1. Protonated forms of pip ($C_4H_{10}N_2$) in acidic area.

gathered for structural determination and further characterization. (54.2% yield). The crystals Anal. Calcd. for **1** (M_w = 3239.38): W, 68.09; B, 0.33; C, 3.70; H, 1.49; N, 2.16%. Found: W, 67.99; B, 0.38; C, 3.64; H, 1.51; N, 2.21%. IR data (KBr, cm^{-1}): 3519 (w), 3461 (w), 3074 (w), 3014 (w), 2952 (w), 2945 (w), 2927 (w), 2837 (w), 2736 (w), 1562 (br), 1440 (m), 1379 (m), 1307 (w), 1191 (w), 1080 (sh), 1002 (w), 958, (m), 900 (s), 806 (vs) and 568 (w). ^{1}H NMR in D_2O: δ 3.444 (s, 2H), and 4.800 (s, 8H)

2.3 *Preparation of 1-CPE*

The construction of **1**-CPE was an easy procedure. The 0.3 g and 0.028 g of graphite and compound **1** powder were blended and converted to homogenous material with an agate mortar and pestle after fifteen minutes. The solid admixture was changed to dough shape by the addition of paraffin (0.4 mL) with a glass rod. The uniform admixture was then put into a glass pipe (with 0.8 mm diameter), and a copper electric cord was located to the back of the electrode for electrical contact. It should be noted that the external surface of the electrode was made uniform for better performance by rotating the electrode surface on the very soft paper.

2.4 *X-ray crystallography*

The structural and crystallographic information of **1** is mentioned in Table S1 (Supplementary Information). The information was collected at 101(2) K on an Xcalibur E diffractometer with Mo K_α monochromated radiation (λ = 0.71073 Å). The resolving and refinement of **1** structure were done on the basis of SHELXS-2014S and SHELXL-2014 program packages with OLEX program, respectively.[24] CCDC No. entrusted in Cambridge Crystallographic Data Center is 1819600. Copies of this information may be obtained gratis from the Director, CCDC, 12 Union Road, Cambridge CB2 1EZ, UK (Tel: 44 (0)1223 762911; e-mail: deposit@ccdc.cam.ac.uk or www: http://www.ccdc.cam.ac.uk).

3. Results and Discussion

3.1 *Synthesis*

The powder form of compound **1** has been grown in the acidified environment (pH = 1.5) consisted of organic protonated ligands (Hpip) and Keggin heteropolyanions after reflux condition (5 h). These units selected to form a solid hybrid material with the aid of electrostatic attraction and hydrogen bonding interactions between heteropolyanions and organic cations produced by proton transfer. To obtain suitable crystals for single-crystal crystallography, a diluted solution including Hpip cations and $[BW_{12}O_{40}]^{5-}$ anions were used. This solution was incubated for a month until appropriate crystals were obtained after slow evaporation of the solvent. The FT-IR spectra comparison between collected crystals and the powder obtained after reflux condition confirmed the similarity of the two materials.

3.2 *Crystal structure explanation*

Crystallographic information of **1** represents that this hybrid forms in the triclinic with P -1 space group. The compound **1** consists of two $[H_5O_2]^+$, two and a half independent Hpip units, four crystallization water molecules and an independent Keggin-type $[BW_{12}O_{40}]^{5-}$ (abbreviated to BW_{12}) cluster (Figure 1a). The BW_{12} cluster represents a normal Keggin structure, including a central BO_4 tetrahedron and four vertex-sharing M_3O_{13} groups, and each M_3O_{13} groups is fixed by three (WO_6) octahedral linked in a triangular arrangement in edge-sharing modes. The bond distance ranges of B-O (1.49–1.54 Å) and W-O (1.70–2.38 Å) are rational in Keggin-type structure, and the angles of O-B-O are between 108 (1)° and 111(1)°, close to tetrahedral 109.28° (Figure S1, Supplementary Information). As shown in Figure 1 b,

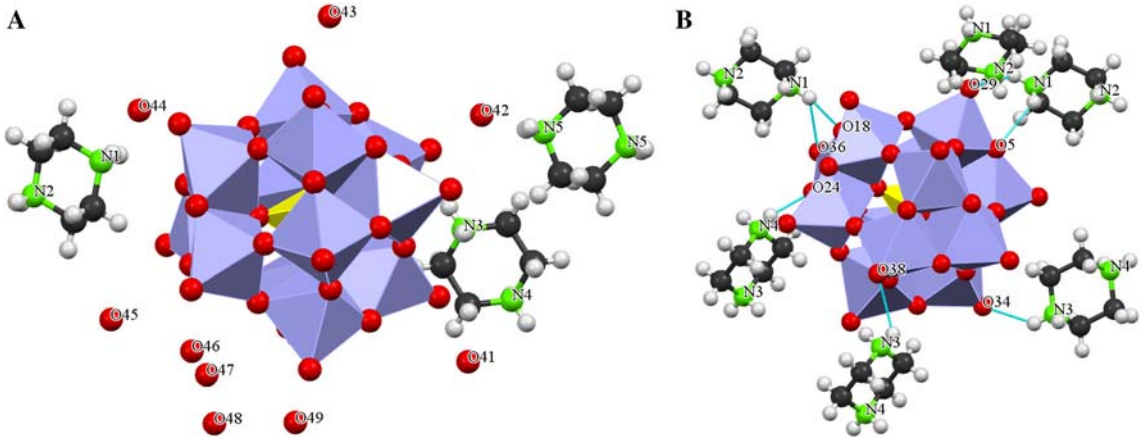

Figure 1. (a) Ball/stick and polyhedral representation of the asymmetric unit of **1**; (b) Each BW_{12} cluster surrounded by six Hpip ligands *via* hydrogen bonds.

each BW_{12} group restricts by six adjoining Hpip ligands and connects to them based on hydrogen bonding. Terminal and bridging oxygen atoms from a BW_{12} cluster connect to each Hpip cation by common hydrogen bonding organized *via* N-H···O interactions. Classic hydrogen bonding organized by these interactions are mainly within the range of 1.954–2.691 Å, indicating the strong hydrogen-bonding interactions.

Three types of Hpip ligands are shown in the **1** structure (Figure 2 a). The first and second groups of Hpip ligands in the connection of three BW_{12} groups to each other play a role through hydrogen bonding, but their difference is in the type of binding atoms. But the third group of Hpip ligands does not bind to BW_{12} anions, and only two types of water molecules are linked to them (Figure 2 a and b). In addition, the type-I placement of Hpip ligands along the (b) axis forms a zigzag-shaped that is repeated in (a) axis direction, and BW_{12} anions are positioned around it (Figure 3). Furthermore, the style placement of Hpip groups is such that they form similar hollows in which the BW_{12} anions are located into them. The size of these hollows, which is about 10–8 Å, corresponds to the approximate diameter of BW_{12} clusters (Figure S2, Supplementary Information). Finally, the four types of Hpip ligands and BW_{12} clusters based on symmetry were observed in the structure of compound **1** (Figure S3, Supplementary Information). It is worth noting that in this figure the BW_{12} clusters are repeatedly layered in a stacked sequence of ABAB and CDCD.

3.3 *FT-IR spectroscopy*

One of the oldest and most used identification tools for chemical compounds is FT-IR spectroscopy applied in this research. $H_5[\alpha\text{-}BW_{12}O_{40}]\cdot nH_2O$ heteropolyacids, compound **1**, and also Hpip cations FT-IR spectra are compared together in Figure S4 a, b and c (Supplementary Information), respectively. Firstly, by comparing the IR spectra of **1** and $H_5[\alpha\text{-}BW_{12}O_{40}]\cdot nH_2O$ the vibration patterns of Keggin-type POM can be demonstrated within 1000–700 cm^{-1} area.[37] By considering to Figure S4 c (Supplementary Information), the specified absorption peaks at 1002, 958, 900 and 806 cm^{-1}, which has proper agreement to Figure S4 a (Supplementary Information), were ascribed to B-O, W-O_t, W-O_b-W and W-O_c-W bonds (O_t, O_b and O_c: terminal, corner-sharing octahedra and edge-sharing octahedra oxygens), respectively. Furthermore, by comparing the b and c parts of Figure S4 (Supplementary Information), it is easy to observe organic functional groups. Thus, the characteristic bands at 3074 and 3014, 2952–2736 range, 1404, 1379 and 1307, 1191 and 1054 cm^{-1}, attributed to the stretching and deformation vibrations of ν(N-H), ν(C-H), ν(C-N-H), ν(C-C), and ν(C-C-N), respectively. Finally, The remarkable red-shift observed in organic groups (N-H) and (C-H) in the compound **1** may be assigned to the hydrogen bonding between Hpip ligands and POM units, which is in appropriate agreement with crystallographic data.

3.4 *^{1}H NMR spectroscopy*

Due to the organic Hpip ligands, the ^{1}H NMR spectrum of compound **1** was also studied (Figure S5, Supplementary Information). As shown in this figure, the presence of CH_2 groups in the Hpip ligands were demonstrated by the appearance of a characteristic peak in the 4.8 ppm area which is compatible against Hpip ^{1}H NMR spectrum.[38] Because of hydrogen bonds between Hpip and BW_{12} units, CH_2 peak moves to almost 2 ppm to downfield. Furthermore, protons of NH groups,

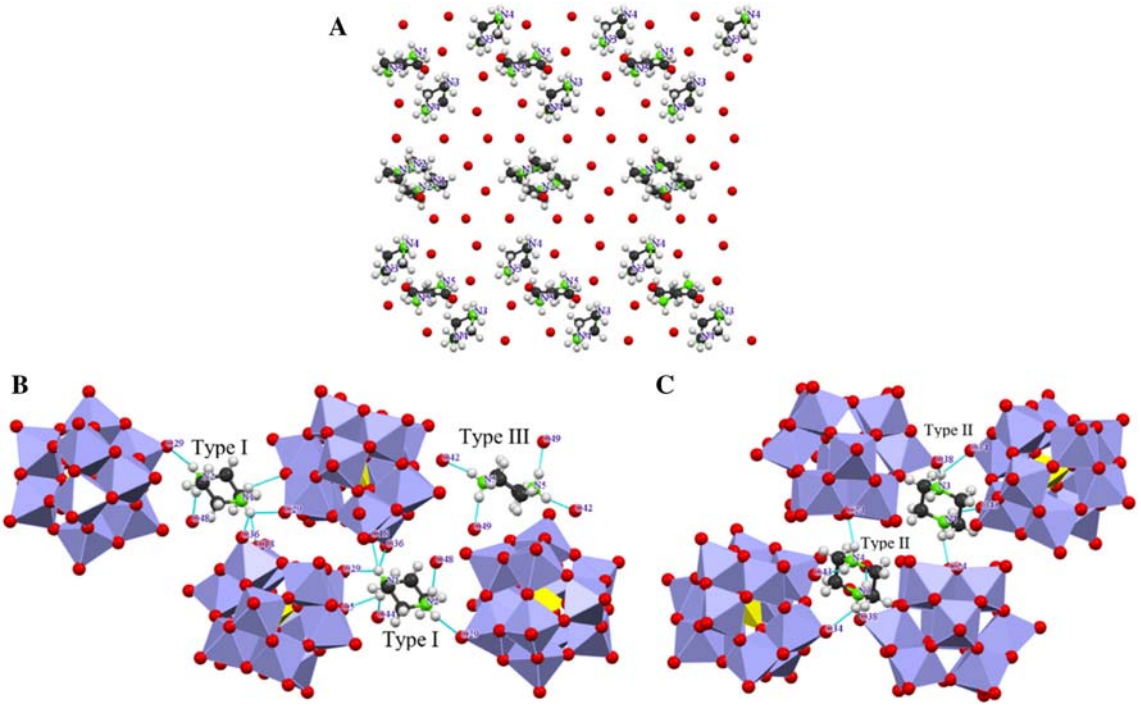

Figure 2. (a) The 2D view of three types of Hpip ligands based on spatial arrangement; (b) and; (c) The 2D view of three types of Hpip ligands based on various connections.

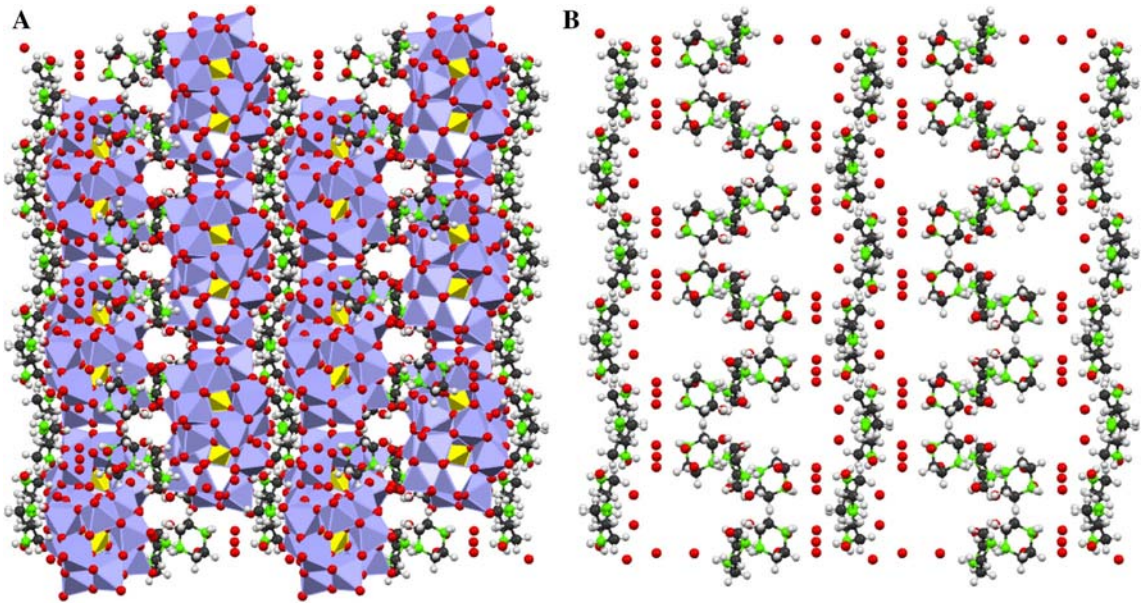

Figure 3. (a) The zigzag-shaped of **1** based on type-I placement of Hpip ligands along the (b) axis with POMs; (b) and without POMs.

appeared in the 3.5 ppm area, do not displace by deuterium since these protons are captive in hydrogen bonds.

3.5 *PXRD analysis*

One of the routine methods that can be used to investigate the phase structure of chemical compounds as well as the particle size is the PXRD analysis. As shown in Figure 4, the similarity between diffraction locations in simulated and experimental patterns of compound **1** represents the crystalline nature and appropriate phase purity of the product. Moreover, the characteristic diffraction of Keggin-type structure are still observed in the compound **1** pattern which shows the existence of BW_{12} units in this compound.[39] In

addition, after five photocatalytic activity tests, the PXRD pattern of compound **1** is almost identical to that of the as-prepared sample (Figure 4).

The average particle size measurement is another result that can be obtained from the PXRD spectrum. By using the Debye-Scherrer formula, the mean crystal measure of **1** was calculated around 42.46 nm (peak position is [2θ°] = 8.1040).[40] Moreover, Williamson Hall method is yet another and more trustworthy way to compute the diameter extent of particles.[41] By using this way, the mean crystal measure of the **1** is 41.3 nm.

3.6 *FESEM study*

FESEM has been used to examine three important factors surface crystallography (i.e., the surface formation of atoms), surface morphology (surface structural features based on shape and size), and surface composition (the composition of surface in term of elements and compounds).

The surface features of the **1** were checked by using FESEM (Figure 5 a, b). As it is obvious from this figure, the appearance of **1** is nanosheet like and extremely alike in essence. In addition, the measure of nano-sheets is almost 45–55 nm which is consistent with the results of PXRD calculations. Eventually, the presence of N, B, W, C and O atoms are clarified by the EDX analysis (Figure 5 c).

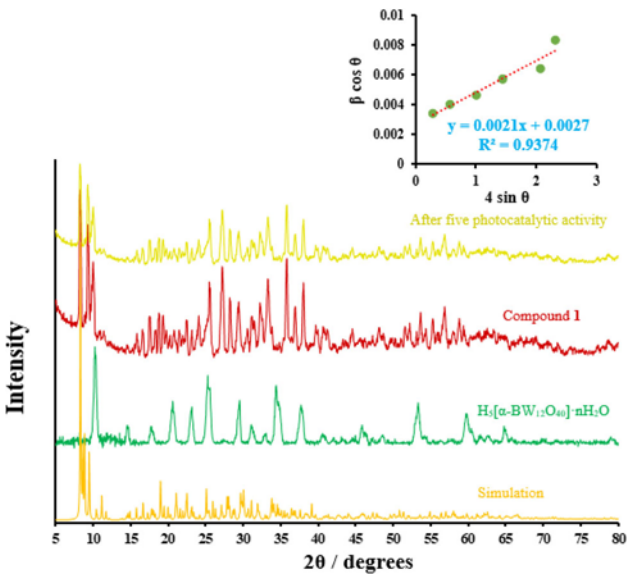

Figure 4. The PXRD patterns of compound **1** simulation (orange line), $H_5[BW_{12}O_{40}]\cdot nH_2O$ (green line), compound **1** as-synthesized (red line) and yellow line (after five photocatalytic processes).

3.7 *TGA-DTA analysis*

The behavior of OIH-POMs during heat treatment can be examined by thermogravimetric and differential thermal analysis (TG-DTA). By considering to thermograms (Figure S6, Supplementary Information), the TG analysis curve of compound **1** shows triple contiguous weight reduction steps. The initial weight reduction is 1.3% (calcd. 1.47%) between 30–200 °C, related to the reduction of four non-coordinated water molecules. The weight decline breakup of 2.5 coordinated Hpip ligands occurred between 200 and 500 °C is about 4.69% (calcd. 4.8%). With increasing temperature, the third weight reduction upper 500 °C is ascribed to the destruction of the POM units.

The three exothermic peaks indicated in DTA curve at 80 and 320, 400 °C are related to the reduction of non-coordinated H_2O molecule and Hpip units, respectively. And also, two endothermic peaks at 600 and 660 °C are attributed to the Keggin units decompositions.

3.8 *The electrochemical behavior*

Because polyoxometalates are stable in acidic media versus neutral and basic solutions, 0.5 M Na_2SO_4/H_2SO_4 (pH = 2.5) buffer aqueous solution has been selected for the electrochemical behavior study of compound **1** (Figure S7 a, Supplementary Information).[42] The existence of four cathodic waves in the negative potentials E = −0.482 (wave I), −0.567 (wave II), −0.661 (wave III) and −0.774 V (wave IV) are related to tungsten centers.[43] The electrochemical behavior of POMs is extremely affected by changes in $[H]^+$ concentration since the redox process of POMs in the acidic environment is attended by protonation. Therefore, the electrochemical behaviors of **1** compound have been assessed in Na_2SO_4/H_2SO_4 buffer solutions at four pH amounts (pH = 1, 1.5, 2 and 2.5). By this assessment, it can be concluded that, by decreasing the concentration of proton in the process environment, the reduction of the **1** compound will be difficult, because the reduction potentials have a negative trend (Figure S7 b, Supplementary Information). In addition, the linear correlation between pH media and redox potential (in each wave) with different slopes show the amount of electron displacement. Waves that are close to the theoretical value −118 mV/pH for $2e^-/2H^+$ (the slope lines of wave III, and IV are −106.2 and −115.4 *mV*/pH respectively), confirming two protons to the two-electron reduction for tungsten elements. However, the slopes for I and II waves (−77.6 and

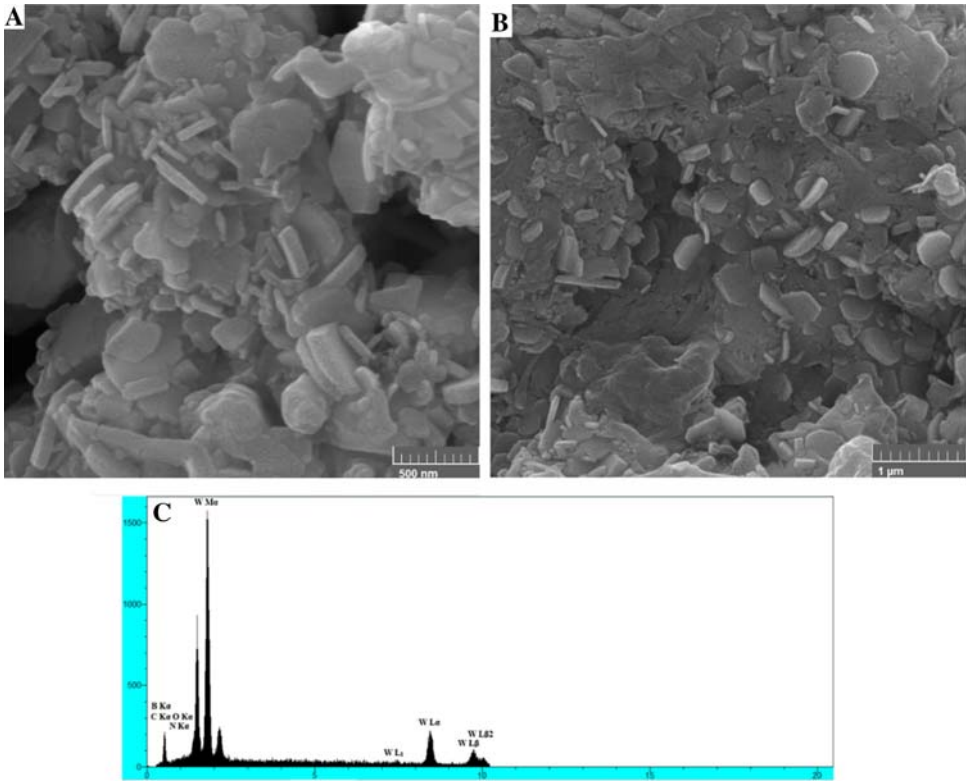

Figure 5. (a) and (b) FE-SEM pictures of **1** hybrid; (c) EDX template of **1** hybrid.

−77.8 *mV*/pH respectively) propose various grades of protonation accompanied by this redox reaction (Figure S7 b, inset, Supplementary Information).[6]

3.9 *Electrocatalytically activity*

As was studied in the past two decades, the application of OIH-POMs in the electrocatalytic reduction of nitrite ion has been considered by researchers extensively because a large overpotential is not necessary for direct electroreduction of nitrite.[44–46] So, the electrocatalytic activity of compound **1** has been regarded in this investigation. The electrocatalytic properties of **1**-CPE in the reduction of nitrite to ammonia ($NO_2^- + 8H^+ + 6e \rightarrow NH_4^+ + 2H_2O$) was studied (Figure 6 a). It is absolutely clear that upon excessing small values of NO_2^- ion (NO_2^- concentration = 0.25, 0.5, 1, 1.5, 2, and 2.5 mM), the reduction current at **1**-CPE increased remarkably. It was showed that **1**-CPE has electrocatalytic characteristics in nitrite reduction. Furthermore, the electrocatalytic efficiency (CAT) of **1**-CPE is evaluated based on the general CAT formula [CAT = 100 × $\{I_p(POM, NaNO_2) - I_p(POM)\}/I_p(POM)$, where $I_p(POM)$ and $I_p(POM, NaNO_2)$ are the cathodic peak currents in the existence and the lack of presence of nitrite ion, respectively].[47] Based on calculations (Table S2, Supplementary Information), the maximum value of CAT (900%) were observed in wave I, among the reduction waves of **1**-CPE at pH = 2.5 (Figure 7 b).

3.10 *Photocatalytic properties*

One of the environmental pollution factors is the decomposition of the organic dye that enters the environment through factories sewage.[48] Therefore, scientists have investigated a variety of catalysts for the elimination of these organic matters, among which OIH-POMs have shown good performance.[49] For this reason, in this paper, we evaluated the photocatalytic activity of **1** compound on the MB degradation.

The MB photodegradation was assessed under visible-light irradiation as follows: the **1** powder (40 mg) was scattered in 50 mL of a 20 ppm (C_0) MB in a beaker by ultrasonic for a half hour. After that, this suspension was unendingly stirred in the darkroom for a half-hour to ensure the adsorption/desorption equilibrium on the catalysts. Then, the mixture was affected under visible-light irradiation from a 200 W LED (light-emitting diode) lamp. After 2, 4, 8, 12, 16, 20 and 24 min, 0.5 mL samples were taken out and the catalyst separated several times by centrifugation.

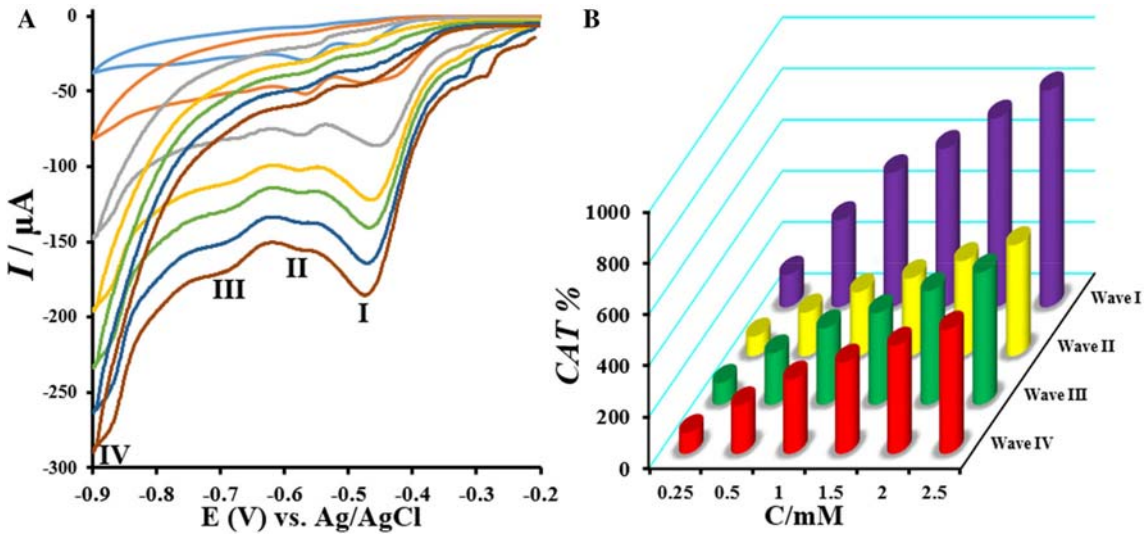

Figure 6. (a) Cyclic voltammograms (scan rate: 100 mV/s) for the electrocatalytic activity of **1** in various addition of NO_2^- (from top to bottom: NO_2^- concentration = 0.25, 0.5, 1, 1.5, 2, and 2.5 mM); (b) Chart of the CAT *vs* concentration of the NO_2^-.

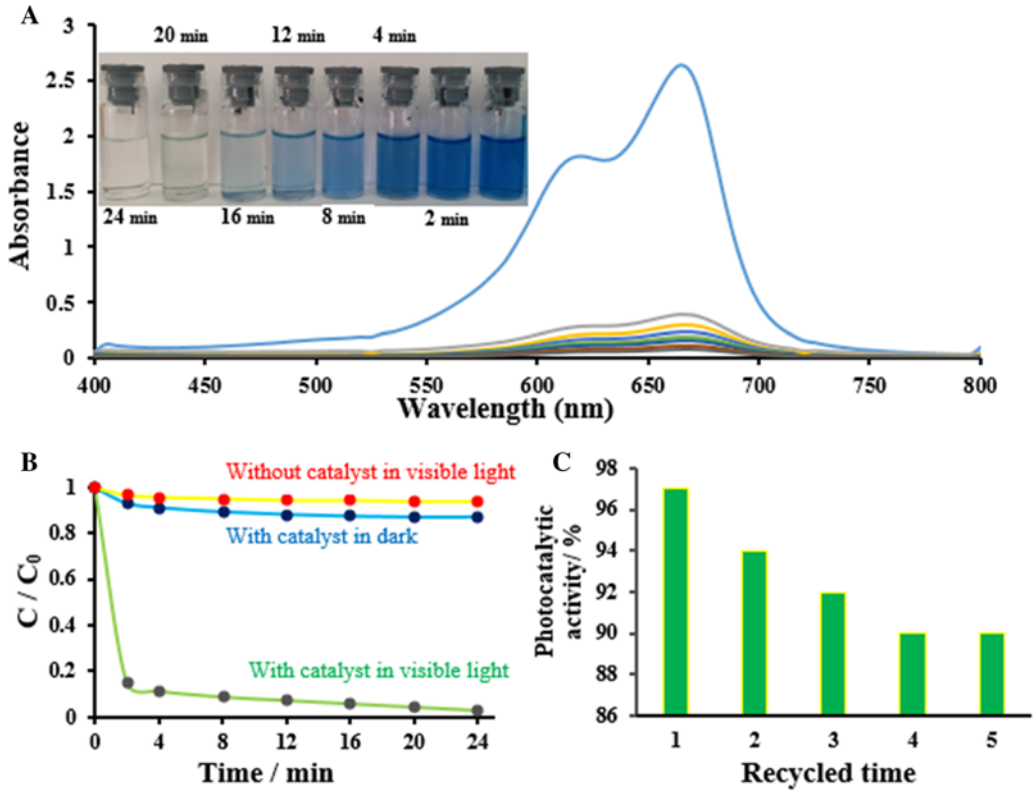

Figure 7. (a) UV-vis adsorption variations seen for MB solutions as a function of visible-light irradiation time for **1** as catalyst; (b) time dependence MB concentration of **1** (green line), photocatalytic investigation of **1** in dark (blue line), the decolorization of MB without catalyst (yellow line); (c) the reusability investigation of compound **1** as catalyst.

The concentration of MB in the reaction media (C_t) was calculated by absorbance measuring at λmax (= 664 nm). The absorption peak of MB declined from 2.63 to 0.077, under visible light illumination (Figure 7 a). As observed in Figure 7 b, the relative absorbance of MB (C_t/Co) versus the reaction time (t) was plotted. The remarkable changes observed in Mb concentration indicate that this organic color has been damaged by the effects of visible light and, of course, catalyst **1**. The results show that 97.08% of MB has been decomposed after only 24 min of visible-light irradiation (Figure 7 b,

green line). Moreover, to study the effect of light and catalyst 1 on the MB degradation, two tests were assessed. The electrocatalytic effect of compound **1** in dark condition was presented such that the decolorization of MB was small (12.93%) (Figure 7 b, blue line). The second test showed that MB decolorization in visible-light irradiation without catalyst was 6.09% (Figure 7 b, yellow line). Finally, the performance of catalyst **1** was maintained as a light photocatalyst was studied after recycled five times. The comparison between the PXRD patterns of **1** before the catalytic process and after five photocatalytic tries displays no clear variations. It also shows that **1** as a heterogeneous catalyst was stable in the catalytic process (Figure 4). The catalytic activity of **1** only slightly decreased after five times of usage (Figure 7 c). The following was done to check the stability of the catalyst: after each catalytic process, the catalyst was collected from the reaction media, purified several times with ethanol and distilled water to remove physisorbed particles, and then dried to prepare for another run.

4. Conclusions

In summary, a new inorganic-organic hybrid, based on the Keggin ions ($BW_{12}O_{40}^{5-}$), was prepared in reflux condition and identified by chemical identification devices. Compound **1** consists of the combination of organic and inorganic groups based on hydrogen bonding between amine units and POM oxygens. There are three types of Hpip ligand in compound **1** that differ from each other according to their type of bonding, and, of course, the configuration of these ligands leads to the formation of cavity shapes and zigzag form in compound **1**. In addition, compound **1** exhibits remarkable electrocatalytic and photocatalytic activities for the reduction of nitrite ion and degradation of MB respectively. Furthermore, the photo-catalyst was effortlessly recycled by centrifugation technique and used again without any noticeable loss of activity after five times.

Supplementary Information (SI)

Additional figures and tables are available at www.ias.ac.in/chemsci.

Acknowledgements

The author thanks the Research Council of Hakim Sabzevari University and Tsinghua University for partial support of this work.

References

1. Han Z, Gao Y, Zhai X, Peng J, Tian A, Zhao Y and Hu C 2008 Self-process-programmed structural diversity in supramolecular assembly based on polyoxometalate anion and halogen-substituted bipyridine cation *Cryst. Growth Des.* **9** 1225
2. Dolbecq A, Dumas E, Mayer C R and Mialane P 2010 Hybrid organic-inorganic polyoxometalate compounds: from structural diversity to applications *Chem. Rev.* **110** 6009
3. Misra A, Kozma K, Streb C and Nyman M 2019 Beyond charge balance: counter-cations in polyoxometalate chemistry *Angew. Chem. Int. Edit.* **59** 596
4. Shakeela K, Silpa G, Rayala S K and Rao G R 2018 Polyoxometalate entrapped caprolactam gels and their cytotoxicity study *J. Chem. Sci.* **130** 107
5. Amanchi S R, Patel A and Das S K 2014 Polyoxometalate coordinated transition metal complexes as catalysts: Oxidation of styrene to benzaldehyde/benzoic acid *J. Chem. Sci.* **126** 1641
6. Zonoz F M 2016 Electrochemistry investigation of the monolacunary and their transition metal substituent Keggin-type polyoxometalates *Electrocatalysis* **7** 215
7. Liu W-J, Dong L-Z, Li R-H, Chen Y-J, Sun S-N, Li S-L and Lan Y-Q 2019 Different protonic species affecting proton conductivity in hollow spherelike polyoxometalates *ACS Appl. Mater. Interf.* **11** 7030
8. Liu L, Wang B, Lv J H, Yu K, Wang L, Zhang H, Wang S and Zhou B B 2017 One-step synthesis of two Wells–Dawson arsenotungstate hybrids via M–O–M bridges for efficient adsorption and selective separation of organic pollutants *CrystEngComm* **19** 5653
9. Varghese C, Shunmugasundaram A, Murugesan R and Abalan T J 2002 EPR investigations of electron transfer in one-electron reduced α-1,4$K_5[PV_2W_{10}O_{40}].3H_2O$ *J. Chem. Sci.* **114** 75
10. Kaczmarek A M 2018 Eu^{3+}/Tb^{3+} and Dy^{3+} POM@MOFs and 2D coordination polymers based on pyridine-2, 6-dicarboxylic acid for ratiometric optical temperature sensing *J. Mater. Chem. C* **6** 5916
11. Gupta R, Hussain F, Sadakane M, Kato C, Inoue K and Nishihara S 2016 Lanthanoid template isolation of the α-1, 5 Isomer of Dicobalt (II)-substituted Keggin type phosphotungstates: syntheses, characterization, and magnetic properties *Inorg. Chem.* **55** 8292
12. Gonçalves C E, Laier L O, Cardoso A L and da Silva M J 2012 Bioadditive synthesis from $H_3PW_{12}O_{40}$-catalyzed glycerol esterification with HOAc under mild reaction conditions *Fuel Proc. Technol.* **102** 46
13. Hou Y, Niu Y, Zhang C, Pang H and Ma H 2017 Two hybrids based on Keggin polyoxometalates and dinuclear copper (II) complexes: syntheses, structures and electrocatalytic properties *J. Chem. Sci.* **129** 1639
14. Taghavi M, Ehrampoush M H, Ghaneian M T, Tabatabaee M and Fakhri Y 2018 Application of a Keggin-type heteropoly acid on supporting nanoparticles in photocatalytic degradation of organic pollutants in aqueous solutions *J. Clean. Prod.* **197** 1447
15. Singhal S, Agarwal S and Kumar A 2019 Isomerization of lighter alkanes by heteropoly acids: a review *J. Catal. Catal.* **2** 1

16. Tan Y-X, Wang F and Zhang J 2018 Design and synthesis of multifunctional metal–organic zeolites *Chem. Soc. Rev.* **47** 2130
17. Ribeiro S, Duarte B, de Castro B, Granadeiro C and Balula S 2018 Improving the catalytic performance of Keggin $[PW_{12}O_{40}]^{3-}$ for oxidative desulfurization: ionic liquids versus SBA-15 composite *Materials* **11** 1196
18. Gopinath S, Kumar P V, Kumar P S M, Arafath K Y, Sivanesan S and Baskaralingam P 2018 Cs-tungstosilicic acid/Zr-KIT-6 for esterification of oleic acid and transesterification of non-edible oils for green diesel production *Fuel* **234** 824
19. Nuryono N, Qomariyah A, Kim W, Otomo R, Rusdiarso B and Kamiya Y 2018 Octyl and propylsulfonic acid co-fixed Fe_3O_4@SiO_2 as a magnetically separable, highly active and reusable solid acid catalyst in water *Mol. Catal.* **475** 110248
20. Jovanović S, Holclajtner-Antunović I, Uskoković-Marković S, Bajuk-Bogdanović D, Pavlović V, Tošić D, Milenković M and Marković B T 2018 Modification of graphene oxide surfaces with 12-molybdophosphoric acid: Structural and antibacterial study *Mater. Chem. Phys.* **213** 157
21. Ross N, Nqakala N, Willenberg S, Sifuba S and Iwuoha E 2019 Electrochemical properties of polyoxometalate ($H_3PMo_{12}O_{40}$)-functionalized graphitic carbon nitride (g-C_3N_4). *Electrocatalysis* **2019** 1
22. Zonoz F M, Jamshidi A and Tavakoli S 2013 Preparation, characterization and electrochemical investigation of a new inorganic–organic hybrid material based on Keggin-type polyoxometalate and organic imidazole cation *Solid State Sci.* **17** 83
23. Yin P, Bayaguud A, Cheng P, Haso F, Hu L, Wang J, Vezenov D, Winans R E and Hao J and Li T 2014 Spontaneous stepwise self-assembly of a polyoxometalate–organic hybrid into catalytically active one-dimensional anisotropic structures *Chem.-A Eur. J.* **20** 9589
24. Bayaguud A, Li J, She S and Wei Y 2017 A simple synthetic route to polyoxovanadate-based organic–inorganic hybrids using EEDQ as an ester coupling agent *Dalton Trans.* **46** 4602
25. Roy S, Sarkar S, Pan J, Waghmare U V, Dhanya R, Narayana C and Peter S C 2016 Crystal structure and band gap engineering in polyoxometalate-based inorganic–organic hybrids *Inorg. Chem.* **55** 3364
26. Lan Y-Q, Li S-L, Shao K-Z, Wang X-L and Su Z-M 2008 Construction of different dimensional inorganic–organic hybrid materials based on polyoxometalates and metal–organic units via changing metal ions: from non-covalent interactions to covalent connections *Dalton Trans.* 3824
27. Han Z-b, Wang X-l, Wang L, Wang E-b, Luan G-y, Hu N-h and Jia H-q 2003 Synthesis, electrocatalytic properties and crystal structure of a new organic-inorganic hybrid constructed from dodecamolybdophosphoric acid and benzotriazole *Chem. Res. Chin. Univ.* **19** 127
28. Cai H, Lü J, Yu K, Zhang H, Wang C, Wang L and Zhou B 2015 Organic–inorganic hybrid supramolecular assembly through the highest connectivity of a Wells–Dawson molybdoarsenate *Inorg. Chem. Commun.* **62** 24
29. Teng C, Xiao H, Cai Q, Tang J, Cai T and Deng Q 2016 Two supramolecular complexes based on polyoxometalates and Co-EDTA units via covalent connection or non-covalent interaction *J. Solid State Chem.* **243** 146
30. Zhou E-L, Qin C, Wang X-L, Shao K-Z and Su Z-M 2016 Assembly of two novel 3D organic–inorganic hybrids based on Keggin-type polyoxometalates: syntheses, crystal structures and properties *CrystEngComm* **18** 6370
31. Wang Q-Q, Wang D-X, Wu Y-L, Zhang Q-P and Xiong H-Y 2018 Synthesis and properties of a new organic-inorganic hybrid compound based on α-Keggin polyoxometalate:$[Cu(Dione)2(H_2O)]_2(SiW_2O)$ *J. Chem. Soc. Pak.* **40** 123
32. Xu L-J, Zhou W-Z, Zhang L-Y, Li B, Zang H-Y, Wang Y-H and Li Y-G 2015 Organic–inorganic hybrid assemblies based on Ti-substituted polyoxometalates for photocatalytic dye degradation *CrystEngComm* **17** 3708
33. Zhao H-Y, Yang B-F and Yang G-Y 2017 Two new 2D organic–inorganic hybrids assembled by lanthanide-substituted polyoxotungstate dimers and copper–complex linkers *Inorg. Chem. Commun.* **84** 212
34. Jamshidi A, Zonoz F M, Wei Y and Maleki B 2018 An organic-inorganic nano-hybrid material containing a mixed-addenda Keggin-type polyoxometalate, piperazine: Synthesis, characterization, its electrochemical investigation *Inorg. Chim. Acta* **477** 233
35. Jiao Y-Q, Qin C, Zang H-Y, Chen W-C, Wang C-G, Zheng T-T, Shao K-Z and Su Z-M 2015 Assembly of organic–inorganic hybrid materials constructed from polyoxometalate and metal–1, 2, 4-triazole units: synthesis, structures, magnetic, electrochemical and photocatalytic properties *CrystEngComm* **17** 2176
36. Wood E 1987 Data for biochemical research by RMC Dawson, DC Elliott, WH Elliott and KM Jones, pp 580. Oxford Science Publications, OUP, Oxford, 1986.£ 35/ $59. ISBN 0-19-855358-7 *Biochem. Edu.* **15** 97
37. https://spectrabase.com/spectrum/6TlncWDFuYz?a=SPECTRUM_6TlncWDFuYz
38. http://sdbs.db.aist.go.jp/sdbs/cgi-bin/direct_frame_top.cgi
39. Mao R, Zhan F, Bu N, Cao Y, Hu P, Gong G and Zhen Q 2016 Room-temperature mechanochemical preparation and electrochemistry properties of polyoxometalate-based inorganic-organic hybrid *Mater. Lett.* **173** 111
40. Zak A K, Majid W A, Abrishami M E and Yousefi R 2011 X-ray analysis of ZnO nanoparticles by Williamson–Hall and size–strain plot methods *Solid State Sci.* **13** 251
41. Javadi F and Tayebee R 2016 Preparation and characterization of ZnO/nanoclinoptilolite as a new nanocomposite and studying its catalytic performance in the synthesis of 2-aminothiophenes via Gewald reaction *Micropor. Mesopor. Mater.* **231** 100
42. Sanchez C, Livage J, Launay J and Fournier M 1983 Electron delocalization in mixed-valence tungsten polyanions *J. Am. Chem. Soc.* **105** 6817
43. Téazéa A, Hervéa G, Finke R G and Lyon D K 2007 α-, β-, and γ-dodecatungstosilicic acids: isomers and related lacunary compounds *Inorg. Synth.* **27** 85

44. Wang Q, Khungwa J, Li L, Liu Y, Wang X and Wang S 2018 Fabrication of polyoxometalate/GO/PDDA hybrid nanocomposite modified electrode and electrocatalysis for nitrite ion, ascorbic acid and dopamine *J. Electroanal. Chem.* **824** 91
45. Li X, Wang Y, Zhou K, Wang Y, Han T and Sha J 2018 Isomeric organic ligand dominating polyoxometalate-based hybrid compounds: synthesis and as electrocatalysts and pH-sensitive probes *J. Coord. Chem.* **71** 468
46. Chen S, Xiang Y, Banks M K, Xu W, Peng C and Wu R 2019 Polyoxometalate-coupled graphene nanohybrid via gemini surfactants and its electrocatalytic property for nitrite *Appl. Surf. Sci.* **466** 110
47. Jamshidi A and Zonoz F M 2017 Synthesis, characterization, electrochemical behavior and electrocatalytical properties towards nitrate and iodate by alcohol solvated Keggin-type polyoxometalate: The effects of weak intermolecular interactions and solvent on electrocatalytical activity *J. Mol. Liq.* **242** 993
48. Ghanbari F and Moradi M 2017 Application of peroxymonosulfate and its activation methods for degradation of environmental organic pollutants *Chem. Eng. J.* **310** 41
49. Tong L, Wang Z, Xia C, Yang Y, Yuan S, Sun D and Xin X 2017 Self-assembly of peptide-polyoxometalate hybrid sub-micrometer spheres for photocatalytic degradation of Methylene Blue *J. Phys. Chem. B* **121** 10566